Histone Variant H3.3 Mediates DNA Repair and cGAS-STING Pathway Activation in Telomere Dysfunction

Chiao-Ming Huang[1] and Liuh-Yow Chen[1,2,3,*]

[1] Molecular and Cell Biology, Taiwan International Graduate Program, Academia Sinica and Graduate Institute of Life Sciences, National Defense Medical Center, Taipei City, Taiwan

[2] Institute of Molecular Biology, Academia Sinica, Taipei, 11529, Taiwan

[3] Lead contact

[*] Correspondence: lyowchen@gate.sinica.edu.tw

ABSTRACT

The telomere damage response is a critical mechanism regulating human aging and disease progression. Deprotected telomeres activate the cytosolic DNA-sensing cGAS-STING pathway; however, the underlying mechanism remains unclear. Here, we discover that histone H3.3 is required for cGAS-STING pathway activation in cells with deprotected telomeres. Expression of the TRF2 dominant-negative mutant, TRF2ΔBΔM, induces telomere dysfunction in fibroblast cells, triggering cGAS-STING pathway activation and growth inhibition. Histone H3.3 depletion significantly reduces this activation, highlighting its critical role in linking telomere deprotection to the cGAS-STING-mediated innate immune signaling. Furthermore, we assess the role of histone H3.3 in telomere fusion. Our finding reveal that histone H3.3 regulates cGAS-STING signaling by controlling telomere fusion. Additionally, depletion of histone H3.3 chaperones, including ATRX, DAXX, and HIRA, inhibits telomere fusion and cGAS-STING pathway activation, underscoring the role of histone H3.3 in telomere maintenance and the DNA damage response. Collectively, our study establishes histone H3.3 as a key regulator of telomere fusion and telomere dysfunction-induced cGAS-STING pathway activation, revealing the correlation between histones and telomeric DNA damage response.

Keywords

Histone H3 Variant H3.3, Telomere Deprotection, Telomere DNA damage response

INTRODUCTION

Telomeres and their associated shelterin proteins are crucial for protecting chromosome ends[1]. Deprotection of telomeres triggers a DNA damage response (DDR), leading to replicative senescence[2-4]. Among the sheltering proteins, telomeric repeat binding factor 2 (TERF2, TRF2) plays a critical role in preventing DDR at chromosome ends. Depletion of TRF2 from telomeres induces cellular senescence and chromosome end-to-end fusion[3], an event that is often found when telomeres are deprotected, particularly under conditions involving dominant-negative TRF2 expression[3]. Previous studies demonstrated that the absence of functional TRF2 activates a DDR mediated by the ataxia telangiectasia mutated (ATM) pathway[3-5]. Upstream components of ATM, including the double-strand break (DSB) sensing complex, the meiotic recombination 11 (MRE11)-radiation sensitive 50 (RAD50)-Nijmegen breakage syndrome 1 (NBS1, NBN) (MRN) complex, play a crucial role in sensing TRF2-dependent telomere deprotection[6-8]. Conversely, downstream effector proteins of ATM, such as Ku protein 70/80 (Ku70/80), ligase IV (LIG4), and x-ray repair cross-complementing 4 (XRCC4), mediate the signaling pathways induced by TRF2 depletion and subsequent telomere fusion[3,9,10]. Together, these findings establish an ATM-dependent mechanism underlying telomere deprotection and the induction of cellular senescence.

Beyond ATM-dependent mechanisms, the cGAS-STING pathway is implicated in telomere dysfunction[11]. In this pathway, cyclic GMP-AMP synthase (cGAS) and stimulator of interferon response cGAMP interactor (STING) collaborate to activate a phosphorylation cascade involving TANK-binding kinase 1 (TBK1), STING, and

interferon regulatory factor 3 (IRF3), which drives the innate immune response by promoting type I IFN transcription[12]. Studies demonstrate that telomere-damaging agents and defective telomere-binding proteins can lead to micronuclei formation, thereby activating the cGAS-STING pathway[11]. Furthermore, evidence supports the involvement of the cGAS-STING pathway in telomere deprotection-induced cellular senescence. For example, chromatin bridges formed during dominant-negative TRF2 expression are processed by three prime repair exonuclease 1 (TREX1)[13], resulting in DNA fragments that activate the cGAS-STING pathway[14]. Similarly, the mutated TRF2, TRF2ΔB induces the formation of extrachromosomal telomere repeats (ECTRs), which are released into the cytosol to trigger the cGAS-STING-mediated innate immune response[15]. Additionally, late-generation mice with deletion of the telomerase RNA component Terc also display senescent signatures along with aberrant STING activation[16]. These findings suggest that telomere deprotection activates both ATM dependent and cGAS-STING pathway, contributing to cellular senescence.

At telomeres, the specific histone variant, histone H3.3, is enriched and plays a crucial role in telomere maintenance[17-19]. Histone H3.3 is deposited in a replication-independent manner by the histone cell cycle regulator (HIRA) complex on euchromatin and by the alpha-thalassemia/mental retardation syndrome X-linked (ATRX)-death domain associated protein (DAXX) complex on heterochromatin, centromeres, and telomeres[18]. While histone H3.3 is known to regulate the active expression of genes[20-24], its function at telomeres remains unclear. Mutations in histone H3.3, such as histone $H3.3^{K27M}$ and histone $H3.3^{G34V}$, are associated with glioblastoma and other telomerase-negative cancers that utilize the alternative

lengthening of telomeres (ALT) pathway[25-28]. ALT, a recombination-based telomere elongation mechanism, is characterized by reduced ATRX expression[28-33] and impaired cGAS-STING pathway activation[15]. Given the role of ATRX-DAXX in depositing histone H3.3 at telomeres, mutations in ATRX, DAXX, and histone H3.3 may alter telomere dynamics and contribute to ALT-associated cancer development[29,34-36]. These observations underscore histone H3.3's potential roles in regulating telomere maintenance.

Previously, we reported that depletion of histone H3.3, ATRX, and DAXX impairs the cGAS-STING pathway activated by ECTRs[15]. Our findings indicated that histone H3.3 participated in the telomere-associated cGAS-STING pathway activation. Additionally, histone H3.3 is involved in DNA damage repair[37], yet the relationship of histone H3.3's roles in regulating DNA damage responses at telomeres and activating the cGAS-STING pathway remains unclear. Here, we demonstrated a role of histone H3.3 in telomere deprotection, the activation of the cGAS-STING pathway, and deprotected telomere-induced cell growth inhibition.

RESULTS

TRF2ΔBΔM expression drives cGAS-mediated growth inhibition

To investigate the signaling pathway induced by the telomeric deprotection, we focused on exploring the downstream cellular response in cells lacking TRF2. We developed an inducible expression system using a Tet-On mechanism to express dominant-negative mutant TRF2ΔBΔM in telomerase-immortalized BJ human fibroblasts (BJ^t), under the control of a tetracycline-dependent promoter. TRF2ΔBΔM, a deletion mutant of TRF2 lacking its N-terminal basic domain and C-terminal DNA binding domain, disrupts the formation of a functional telomere shelterin complex by displacing endogenous TRF2, leading to telomere deprotection and fusion[3]. Upon adding doxycycline (DOX), we observed the expression of myc-tagged TRF2ΔBΔM (Fig. 1A) and the formation of telomere dysfunction-induced foci (TIFs), characterized by the colocalization of phosphorylated histone H2AX (γH2AX) with telomeres (Fig. 1B) in BJ^t cells.

In line with our aims, we observed the activation of cGAS-STING response following TRF2ΔBΔM induction. Notably, STING phosphorylation, a critical event for the cGAS-STING pathway that facilitates the phosphorylation of IRF3 to drive IFN expression[38,39], was detected on day 2 and peaked on day 3 post-DOX treatment, indicating that cGAS-STING pathway was activated (Fig. S1A). This activation correlated with the induction of TRF2ΔBΔM expression (Fig. S1A). Reverse-transcription quantitative polymerase chain reaction (RT-qPCR) revealed upregulated expression of IFN beta (IFNβ) mRNA after induced expression of TRF2ΔBΔM (Fig. S1B). These findings

suggest that induced expression of TRF2ΔBΔM drives downstream responses including the STING phosphorylation and the transcription of IFNβ.

To determine whether cGAS plays a role in STING activation upon TRF2ΔBΔM expression, we depleted it using small interfering RNAs (siRNAs) before DOX induction. Depletion of cGAS inhibited STING phosphorylation and IFNβ transcription in the TRF2ΔBΔM-expressing cells (Fig. 1C, D), supporting the conclusion that TRF2ΔBΔM activates the cGAS-STING signaling cascade to promote IFNβ production. These results are reminiscent of those from previous studies indicating that TRF2 inhibition activates the cGAS-STING pathway[11,15].

Furthermore, previous reports have described telomere deprotection induced by TRF2ΔBΔM expression as a trigger for cell growth arrest[3]. Consistently, we also observed that DOX-induced TRF2ΔBΔM expression in BJ^t cells led to significantly reduced cell growth (Fig. 1E). Since cGAS-STING pathway activation induces IFNβ expression and affects cell proliferation[15], we hypothesized that the cell growth defects associated with TRF2ΔBΔM expression might be driven by cGAS-STING pathway activation. To test this possibility, we transfected BJ^t cells with siRNAs to silence cGAS expression and monitored their subsequent cell growth. Our results demonstrated that cGAS depletion partially rescued the cell proliferation defects of BJ^t cells expressing TRF2ΔBΔM (Fig. 1F), indicating that induction of the cGAS-STING pathway contributes to TRF2ΔBΔM-mediated cell growth defects. Thus, the cGAS-STING pathway exerts a fundamental role in mediating cellular growth impairment due to telomere deprotection.

Histone H3.3 regulates the cGAS-STING-pathway-mediated cell growth inhibition upon telomere dysfunction

Previously, we showed that histone H3.3 and its chaperone, the ATRX-DAXX complex, promote the activation of cGAS-STING pathway[15]. This activation occurs in response to the accumulation of ECTRs following artificially induced telomere excision by another TRF2 mutant, TRF2ΔB, which lacks only the N-terminal basic domain[15]. This finding demonstrates that the release of telomeric DNA into the cytosol, a phenomenon commonly observed in ALT cancers[40-42], activates cGAS-STING pathway. Given that ectopic expression of either TRF2ΔB or TRF2ΔBΔM elicits TRF2 dysfunction, we sought to investigate if histone H3.3 is involved in the cGAS-STING pathway activation driven by TRF2ΔBΔM-induced telomere deprotection. To do so, we used siRNAs to deplete histone H3.3 from BJ^t cells and then examined TRF2ΔBΔM-induced STING phosphorylation and IFNβ production. Our results revealed that histone H3.3 depletion significantly reduced STING phosphorylation and IFNβ expression in BJ^t cells expressing TRF2ΔBΔM (Fig. 2A, B). Furthermore, siRNA-mediated histone H3.3 silencing alleviated the phenotype of defective cell proliferation associated with TRF2ΔBΔM (Fig. 2C). Importantly, the phosphorylation of STING can be rescued by ectopically expressing the siRNA-insensitive H3.3 (Fig. 2D). Collectively, our findings suggest that histone H3.3 mediates cGAS-STING pathway activation and the subsequent cell growth impairment arising from telomere deprotection.

Telomere fusion by non-homologous end joining (NHEJ) promotes cGAS-STING pathway activation

Telomere deprotection resulting from TRF2 deficiency leads to telomere fusion via the NHEJ pathway[3,10,43], which in turn generates micronuclei[11,44] and activates the cGAS-STING pathway[11]. While some studies debate whether micronucleus formation directly triggers cGAS-STING pathway activation[45], we hypothesized that cGAS-STING pathway activation following TRF2ΔBΔM expression may result from telomere fusion. To test this hypothesis, we used siRNAs to silence the expression of the LIG4 and XRCC4, two key proteins that mediate telomere fusion via the NHEJ mechanism[10]. We found that depletion of LIG4 or XRCC4 in BJ^t cells reduced TRF2ΔBΔM-induced telomere fusion, as evidenced by the diminished apparent convergence of telomere signals at chromosome ends (Fig. 3A, B). Furthermore, silencing LIG4 or XRCC4 decreased the formation of abnormal nuclear structures, including nucleoplasmic bridges, nuclear buds, and micronuclei (Fig. 3C, D). Notably, LIG4 or XRCC4 depletion also inhibited STING phosphorylation and IFNβ mRNA induction in BJ^t cells expressing TRF2ΔBΔM (Fig. 4). These results suggest that activation of the cGAS-STING pathway in response to TRF2ΔBΔM expression may be attributable to NHEJ-mediated fusion of deprotected telomeres.

Histone H3.3 mediates DDR and telomere fusion for cGAS-STING pathway activation

As shown above, histone H3.3 plays a role in activating the cGAS-STING pathway in BJ^t cells with deprotected telomeres (Fig. 2). We hypothesized that histone H3.3 contributes to telomere fusion, which in turn influences cGAS-STING pathway activation. To examine this possibility, we silenced histone H3.3 expression in BJ^t cells

by siRNAs and analyzed subsequent telomere fusion and nuclear structural abnormalities following TRF2ΔBΔM induction for two days. Our results demonstrate that depletion of histone H3.3 significantly reduced the number of telomere fusion events and partially reduced the formation of micronuclei, nuclear buds, and nucleoplasmic bridges typically induced by TRF2ΔBΔM expression (Fig. 3). These findings indicate that histone H3.3 is required for NHEJ-mediated telomere fusion following telomere deprotection. Our results reveal that chromosomal and nuclear abnormalities occur on the second day after inducting TRF2 mutant expression. Notably, this precedes the peak cGAS-STING response, which occurs on the third day post-induction of TRF2ΔBΔM expression (Fig. 3, S1). These observations suggest that histone H3.3 orchestrates the downstream response to TRF2ΔBΔM-induced telomere deprotection, including telomere fusion, nuclear abnormalities, and subsequent cGAS-STING pathway activation. Since depletion of cGAS did not rescue TRF2ΔBΔM-mediated telomere fusion or nuclear abnormalities (Fig. 3), cGAS does not appear to directly participate in DNA repair at deprotected telomeres but rather functions downstream of telomere fusion and nuclear abnormalities. Thus, our results suggest that histone H3.3 mediates cGAS-STING activation by promoting NHEJ-mediated repair of deprotected telomeres.

Next, we investigated if histone H3.3 regulates the telomere DDR and thereby controls NHEJ for subsequent cGAS-STING activation. As evidenced above, expression of TRF2ΔBΔM elicited moderate TIF formation (Fig. 1B, 5A-C), indicating that telomere deprotection can trigger a DDR. To determine whether histone H3.3 regulates the telomeric DDR, we treated BJ^t cells with siRNAs to deplete the expression of histone H3.3. Interestingly, we observed that depletion of histone H3.3 also reduced TIF

formation in the TRF2ΔBΔM-expressing cells (Fig. 5A-C), supporting that the role of histone H3.3 in regulating the DDR at deprotected telomeres. These findings underscore the role of histone H3.3 in regulating the TRF2ΔBΔM-induced telomeric DDR.

Since NBS1 is a key component of the MRN complex, we hypothesized that its depletion would impair telomeric DDR. The results showed that TRF2ΔBΔM-induced TIF formation was abolished upon NBS1 depletion (Fig. 5A-C), consistent with the MRN complex playing a role in sensing telomere deprotection to activate a DDR[46]. To investigate whether the MRN complex regulates cGAS-STING activation, we measured IFNβ production in cells treated with the MRN inhibitor, Mirin[47]. Treatment with 25 μM Mirin significantly reduced STING phosphorylation and IFNβ transcription in TRF2ΔBΔM-expressing cells, confirming that MRN is essential for cGAS-STING activation following telomere deprotection (Fig. 5D, E). Our observations further demonstrate that the cellular machinery responsible for telomeric DDR also modulates the activation of cGAS-STING pathway. Collectively, these results indicate that histone H3.3 and MRN complex facilitate DDR activation and NHEJ at deprotected telomeres, thereby priming cells for subsequent cGAS-STING pathway activation.

Histone H3.3's chaperones are required for TRF2ΔBΔM-driven cGAS-STING pathway activation, telomere fusion, and TIF formation

Histone chaperones, including ATRX-DAXX and HIRA, have been shown to mediate the deposition of histone H3.3 on telomeres[18,48]. Anti-silencing function 1 (ASF1) binds histone H3.3-H4 dimers and transfers them to HIRA[48]. To investigate if deposition of

histone H3.3 on telomeres is important for regulating telomere deprotection-induced cGAS-STING activation, we used siRNAs to deplete individual histone H3.3 chaperone proteins, including ASF1, HIRA, ATRX, and DAXX, from BJ^t cells expressing TRF2ΔBΔM. Consistently, depletion of ATRX, DAXX, or HIRA reduced the telomeric distribution of histone H3.3, as evidence by decreased telomeric signals in histone H3.3 chromatin immunoprecipitation (ChIP) assays following siRNA-mediated depletion of ATRX, DAXX, or HIRA siRNAs (Fig. S2). STING phosphorylation and IFNβ expression were reduced upon TRF2ΔBΔM expression in the absence of ATRX or DAXX (Fig. 6A, 6C). Additionally, depletion of HIRA or ASF1 significantly reduced STING phosphorylation and IFNβ expression in TRF2ΔBΔM-expressing cells (Fig. 6B, 6C). Together, these observations indicated that ATRX, DAXX, HIRA, and ASF1 are all required to activate the cGAS-STING response caused by telomere deprotection.

To determine how these histone chaperones regulate downstream responses to telomere deprotection, we assessed telomeric DDR and telomere fusion in cells depleted of ATRX, DAXX, or HIRA. Depletion of ATRX, DAXX, or HIRA reduced the percentages of fused chromatids and TIF formation in TRF2ΔBΔM-expressing BJ^t cells (Fig. 6D, S3), indicating that proper telomeric distribution of histone H3.3 is essential for DDR activation and telomere fusion following telomere deprotection. Thus, histone H3.3 localization at telomeres is essential for DDR activation, telomere fusion, and cGAS-STING pathway activation.

DISCUSSION

Our results reveal a role for histone H3.3 in mediating telomere deprotection-induced activation of the cGAS-STING pathway. Although histone H3.3 deposition at telomeres has been previously documented, its role in telomere dynamics and the DNA damage response remains poorly understood. Notably, mutations in *H3F3A*, the gene encoding histone H3.3, are strongly associated with glioblastoma, a tumor that predominantly relies on the ALT mechanism[28,49]. Our previous work demonstrated that ALT cancer cells lack a functional cGAS-STING-mediated intracellular DNA sensing mechanism and that histone H3.3 and its chaperone contribute to regulating this pathway[15]. Here, we show that histone H3.3 contributes to telomere fusion events and the formation of TIFs in cells with deprotected telomeres (Fig. 3, 5). These findings suggest that histone H3.3 contributes to ALT cancer-associated telomere dysfunctions, including TIF formation, chromosome fusion events, and cGAS-STING pathway activation.

Recent studies have shown that glioblastoma-associated histone H3.3 variants, such as histone $H3.3^{K27M}$ and histone $H3.3^{G34V}$, impair chromosome segregation, trigger genetic instability[25], and regulate ALT-associated features[50]. These findings suggest that ALT-associated histone H3.3 mutations may suppress the DDR, promote genetic instability, and facilitate error-prone genome doubling and rapid cell cycle progression. These mutations may also suppress cGAS-STING activation, dampening the innate immune response and allowing cancer cells to thrive under genomic stress. However, further studies are needed to clarify the relationship between histone H3.3 mutations

and cGAS-STING pathway activity in ALT cancer cells to better understand how these mutations contribute to ALT phenotypes.

ALT cancers maintain telomeres through a telomerase-independent recombination-driven process. Given the link between histone H3.3 and ALT cancers[25-28], we propose that its expression and telomeric deposition influence DNA repair pathway choice, shifting the balance between NHEJ and homologous recombination (HR). Histone H3.3 has been shown to function downstream of the PARP1-CHD2 machinery to promote NHEJ at telomeres[37]. Similarly, the histone H3.3's chaperone molecule, ATRX is active in both NHEJ[33] and HR[51]. In our observations, depletion of histone H3.3 or its chaperones (ATRX, DAXX, and HIRA) reduces telomere fusion events (Fig. 3, 6) and impairs TIF formation (Fig. 5, S3), underscoring their importance in telomere repair. Since ALT phenotypes depend on HR, we propose that mutations in histone H3.3 or its chaperones disrupt NHEJ while enhancing HR, thereby supporting ALT telomere maintenance. It will be important to establish in the future how histone H3.3 localization and chaperone interactions mediate this switch.

Telomere fusion has been proposed as a mechanism to counteract telomere shortening[52,53]. However, our findings reveal that telomere fusion also activates the cGAS-STING pathway, which may impair cell growth. This scenario is evidenced by the impairment of cGAS-STING activation we detected upon depletion of the DNA repair proteins LIG4 and XRCC4 (Fig 4). Furthermore, cGAS depletion rescues the growth inhibition induced by telomere deprotection (Fig. 1E, F), suggesting that telomere fusion promotes cellular senescence via cGAS-STING pathway activation. Interestingly, our findings indicate that cGAS-STING activation occurs in a pulsatile

manner following telomere deprotection (Fig. S1). Thus, telomere fusion appears to trigger rapid but transient activation of this pathway under telomeric stress. Notably, transient activation of the cGAS-STING pathway by TRF2ΔBΔM expression is sufficient to inhibit cell growth (Fig. 1E, F). These findings reveal a novel role for telomere fusion in transient cGAS-STING pathway activation and cell growth regulation. Future studies should explore the mechanisms underlying this temporal control and its broader implications. Overall, our results highlight the essential role of histone H3.3 in deprotected telomere-driven cGAS-STING signaling and provide new insights into its underlying mechanisms.

RESOURCE AVAILABILITY

Lead contact

Requests for further information and resources should be directed to and will be fulfilled by the lead contact, Liuh-Yow Chen (lyowchen@gate.sinica.edu.tw).

Materials availability

This study did not generate new unique reagents.

Data and code availability

Original Western blot images and microscopy data reported in this paper will be shared by the lead contact. Any additional information required to reanalyze the data reported in this paper is available from the lead contact upon request.

ACKNOWLEDGEMENT

We thank the Imaging Core of the Institute of Molecular Biology (IMB), Academia Sinica, for technical support. We also thank Nithila Joseph in our lab and John O'Brien for assistance with English editing. This project is supported by grants from Academia Sinica (AS-GCP-113-L02) and the Ministry of Science and Technology (111-2311-B-001-013).

AUTHOR CONTRIBUTIONS

Conceptualization, C.-M. H. and L.-Y. C.; methodology, C.-M. H.; analysis, C.-M. H.; investigation, C.-M. H.; resources, L.-Y. C.; writing – original draft, C.-M. H. and L.-Y. C.; writing – review and editing, C.-M. H. and L.-Y. C.; funding acquisition, L.-Y. C.;

supervision, C.-M. H. and L.-Y. C.

DECLARATION OF INTERESTS

The authors declare no competing interests.

FIGURES

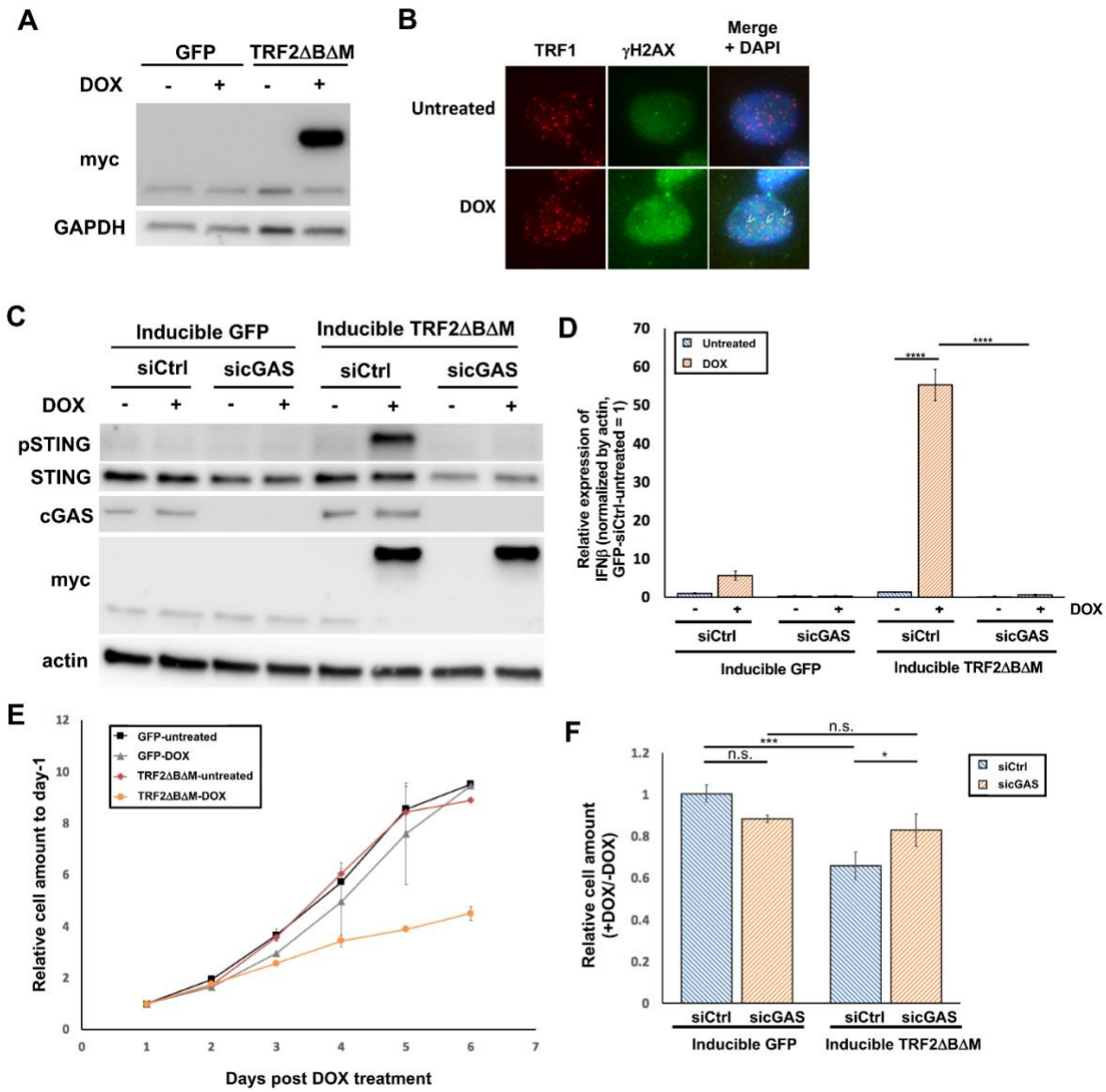

Figure 1. Expression of TRF2ΔBΔM triggers cGAS-STING pathway activation and cGAS-mediated growth inhibition.

BJ^{t} cells were separated into untreated and treatment groups, and then 25 ng/ml doxycycline (DOX) was mixed into the culture medium of the treatment group to induce expression of TRF2ΔBΔM. (**A**) Ectopic expression of myc-tagged TRF2ΔBΔM and GAPDH and was determined by Western blotting. (**B**) Immunostaining for γH2AX and TRF1 was performed on day 4 after DOX treatment. Representative

images stained for γH2AX (green) and TRF1 (red). White arrowheads indicate representative colocalized signals of TRF1 and γH2AX. For silencing the expression of cGAS, siRNAs were added twice, i.e., at 60 h and 12 h before inducing TRF2ΔBΔM. (**C**) Protein levels of STING phosphorylated at residue S366 (pSTING), STING, cGAS, myc, and actin were determined by Western blotting. (**D**) The expression level of IFNβ mRNA was determined by RT-qPCR. qPCR experiments represent the mean ±SD of three technical repeats. (**E**) Numbers of cells surviving under the indicated conditions were determined by counting the DAPI signals in the culture dishes. Cell numbers were normalized to day 1 after treatment for each experiment. Data represent the mean ±SD of three biological repeats. (**F**) BJ^t cells inducibly expressing GFP or TRF2ΔBΔM and respective controls were treated with or without 25 ng/ml DOX. Surviving cells were counted 4 days later. Statistical analysis was conducted using one-way ANOVA. n.s. represents no significant differences, * p-value < 0.05, *** p-value <0.001, and **** p-value < 0.0001.

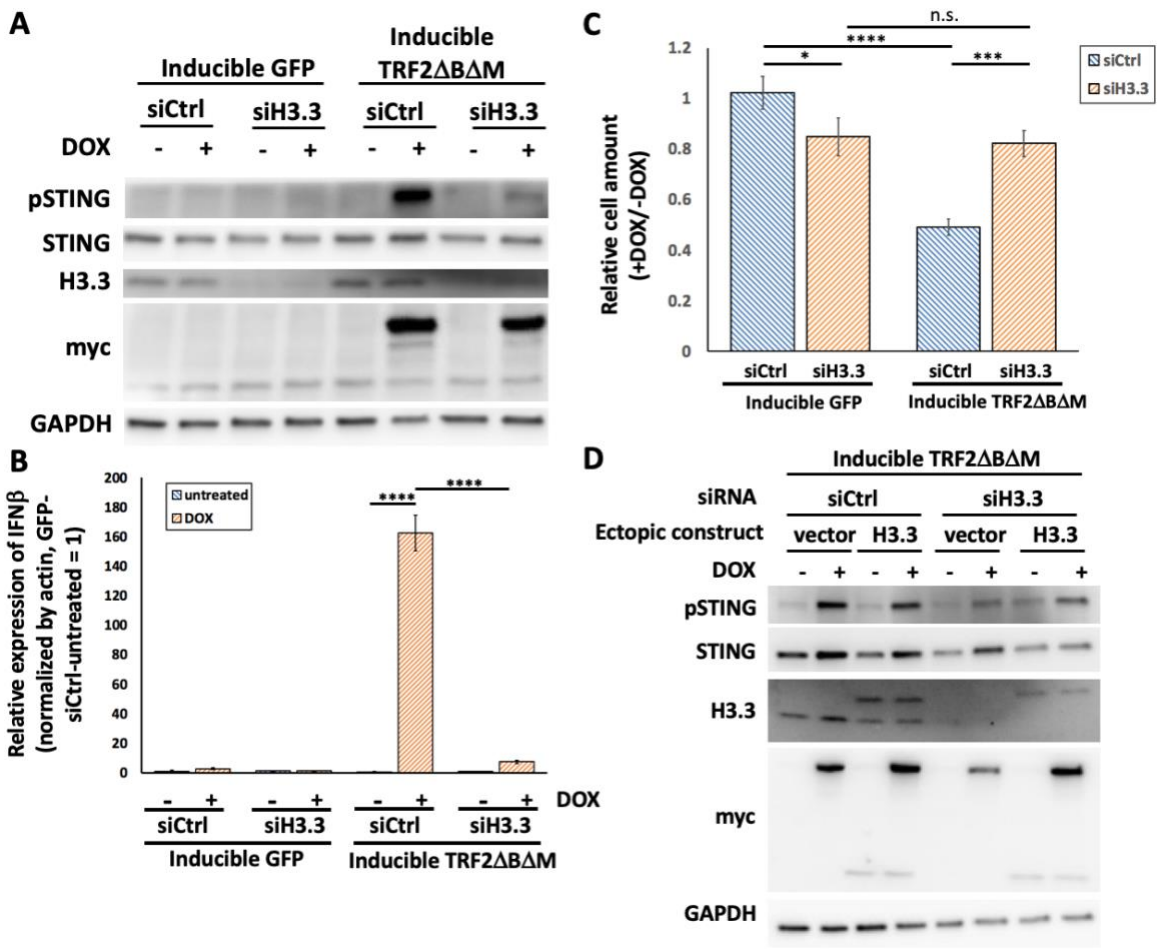

Figure 2. Depletion of H3.3 impairs cGAS-STING pathway activation and rescues growth defects due to the expression of TRF2ΔBΔM.

(**A**) BJ^{t} cells stably expressing GFP or myc-tagged TRF2ΔBΔM were established. siRNAs were then added at two different times, i.e., at 60 h and 12 h before inducing TRF2ΔBΔM expression through doxycycline (DOX). Samples were cultured for 2.5 days to investigate the cGAS-STING signaling response. Protein levels of phosphorylated STING (pSTING), STING, H3.3, myc, and GAPDH were determined by Western blotting. (**B**) mRNA expression levels of IFNβ were determined by RT-qPCR. qPCR experiments represent the mean ±SD of three technical repeats. (**C**) Numbers of cells in the DOX+ or DOX- treatment groups were counted to evaluate cell growth 4 days later. Data represent the mean ±SD of three biological repeats. (**D**)

A siRNA-insensitive H3.3 construct was introduced into cells via viral vectors and ectopically expressed. Protein levels of phosphorylated STING (pSTING), STING, H3.3, myc, and GAPDH were then determined by Western blotting. Statistical analysis was conducted using one-way ANOVA. n.s. represents no significant differences, * p-value < 0.05, *** p-value <0.001, and **** p-value < 0.0001.

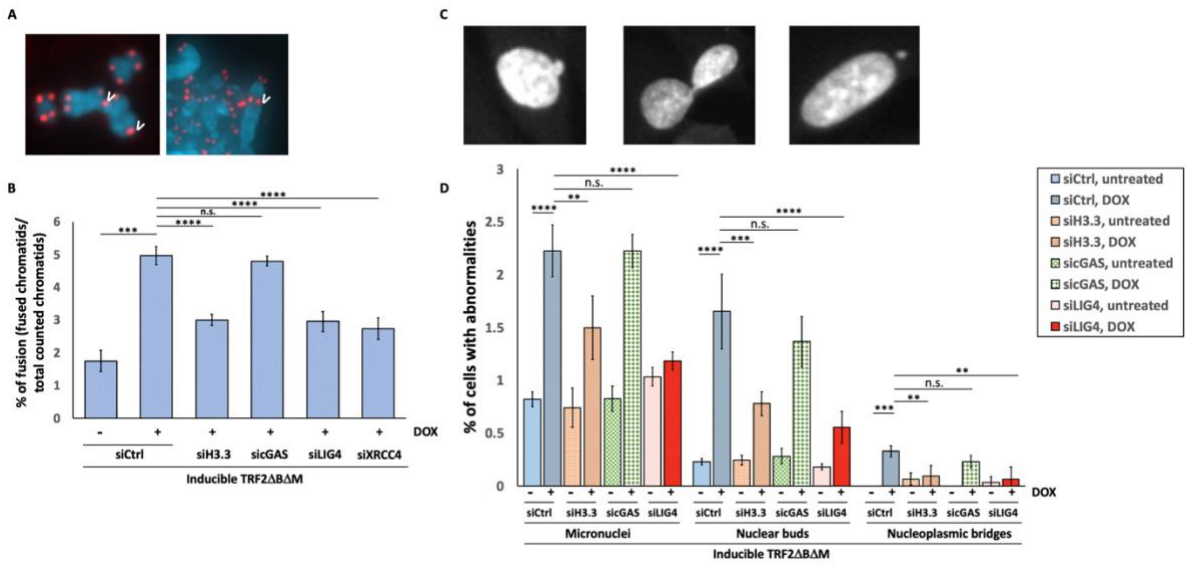

Figure 3. Depletion of H3.3 expression limits telomere-to-telomere fusion events and the formation of nuclear abnormalities.

BJ^{t} cells were treated with siRNAs including siCtrl, siH3.3, sicGAS, siLIG4, and siXRCC4 at 60 h and 12 h before DOX treatment to induce expression of TRF2ΔBΔM for 24 h. Cells were arrested using 0.1 μg/ml Demecolcine for another 24 h, and then spread on a slide to visualize telomere-to-telomere fusion events by staining with TelC probes. (**A**) Representative images of telomere fusion events (white arrows). (**B**) Quantitative results for telomere fusion events were calculated from >2000 chromosomes for each sample. Data represent mean ±SD of three biological repeats. (**C**) Representative cells images of siRNA-treated cells on day 2 after DOX treatment. For each group, >1,000 nuclear images were acquired and counted to determine percentages of the indicated nuclear abnormalities. Representative images are shown for a nuclear bud (left), a nucleoplasmic bridge (middle), and a micronucleus (right). (**D**) Quantitative results for nuclear abnormalities. Data represent the mean ±SD of three technical repeats. Statistical analysis was conducted using one-way ANOVA. n.s. represents no significant differences, ** p-value < 0.01, *** p-value <0.001, and **** p-value < 0.0001.

433

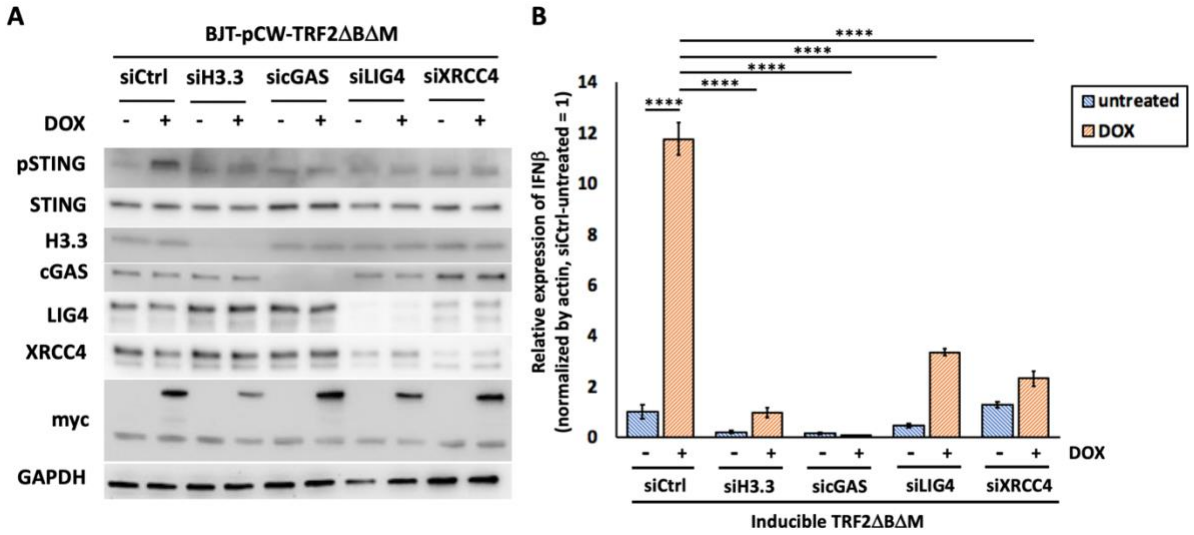

Figure 4. Depletion of LIG4 and XRCC4 disrupts activation of the cGAS-STING response.

BJ^t cells inducibly expressing myc-tagged TRF2ΔBΔM were treated with siRNAs at 60 h and 12 h before doxycycline (DOX) treatment. To correlate telomere fusion events and nuclear abnormalities, treated cells were lysed on day 2 after DOX treatment. (**A**) Protein levels of phosphorylated STING (pSTING), STING, H3.3, cGAS, LIG4, XRCC4, myc, and GAPDH were determined by Western blotting. (**B**) mRNA expression levels of IFNβ were determined by RT-qPCR. qPCR experiments represent the mean ±SD of three technical repeats. Statistical analysis was conducted using one-way ANOVA. **** p-value < 0.0001.

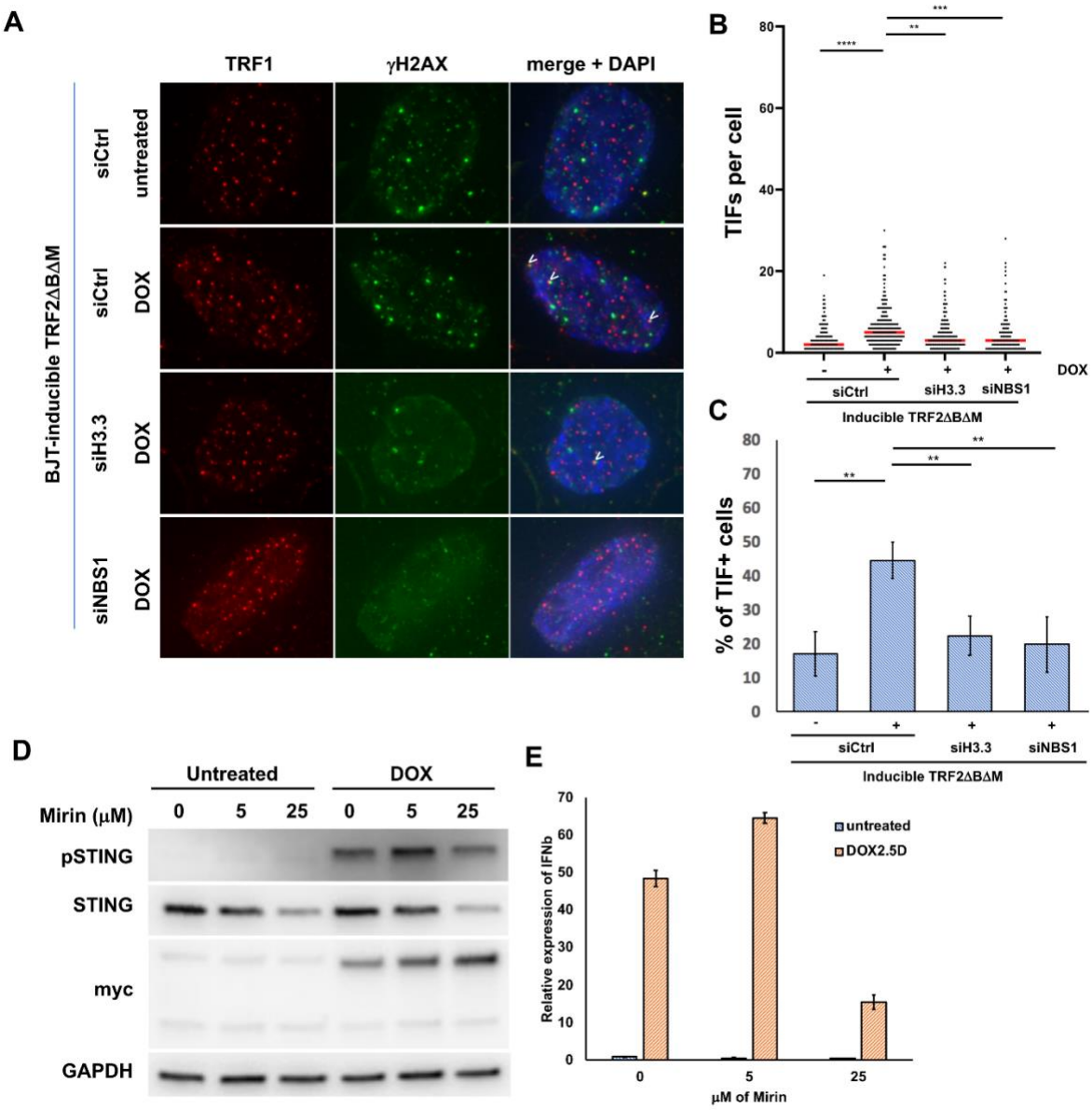

Figure 5. Depletion of H3.3 expression limits TIF formation.

BJ^t cells were treated with siRNAs including siCtrl, siH3.3, and siNBS1 at 60 h and 12 h before inducing stable expression of TRF2ΔBΔM or TPP1ΔRD through 2.5 ng/ml DOX treatment. (**A**) Immunostaining for γH2AX and TRF1 was performed on day 2 after DOX treatment. Representative images stained for γH2AX (green) and TRF1 (red). White arrowheads indicate representative colocalized signals of TRF1 and γH2AX, which are defined as TIFs, in the cells. (**B**) Numbers of TIFs per cell for the different treatment groups. Each dot represents the TIF count per cell. Red lines

indicate the median value for each group. The data represent three biological repeats, with 70-120 cells counted in each repeat, and each experimental group represents 250-330 cells. (**C**) Percentages of cells harboring >5 TIFs. More than 100 cells were quantified for each sample in each repeat. BJ^t cells inducibly expressing either TRF2ΔBΔM were treated with 0, 5, or 25 μM of MRN complex inhibitor, Mirin. Total RNA and protein samples are collected after doxycycline treatment for 2.5 days. (A) Protein levels of phosphorylated STING (pSTING), STING, myc, and GAPDH were determined by Western blotting. (B) Relative expression levels of IFNβ mRNA in each sample group were determined by qPCR. qPCR experiments represent the mean ±SD of three technical repeats. Data represent mean ±SD of three biological repeats. Statistical analysis was conducted using one-way ANOVA. ** p-value < 0.01, *** p-value <0.001, and **** p-value < 0.0001.

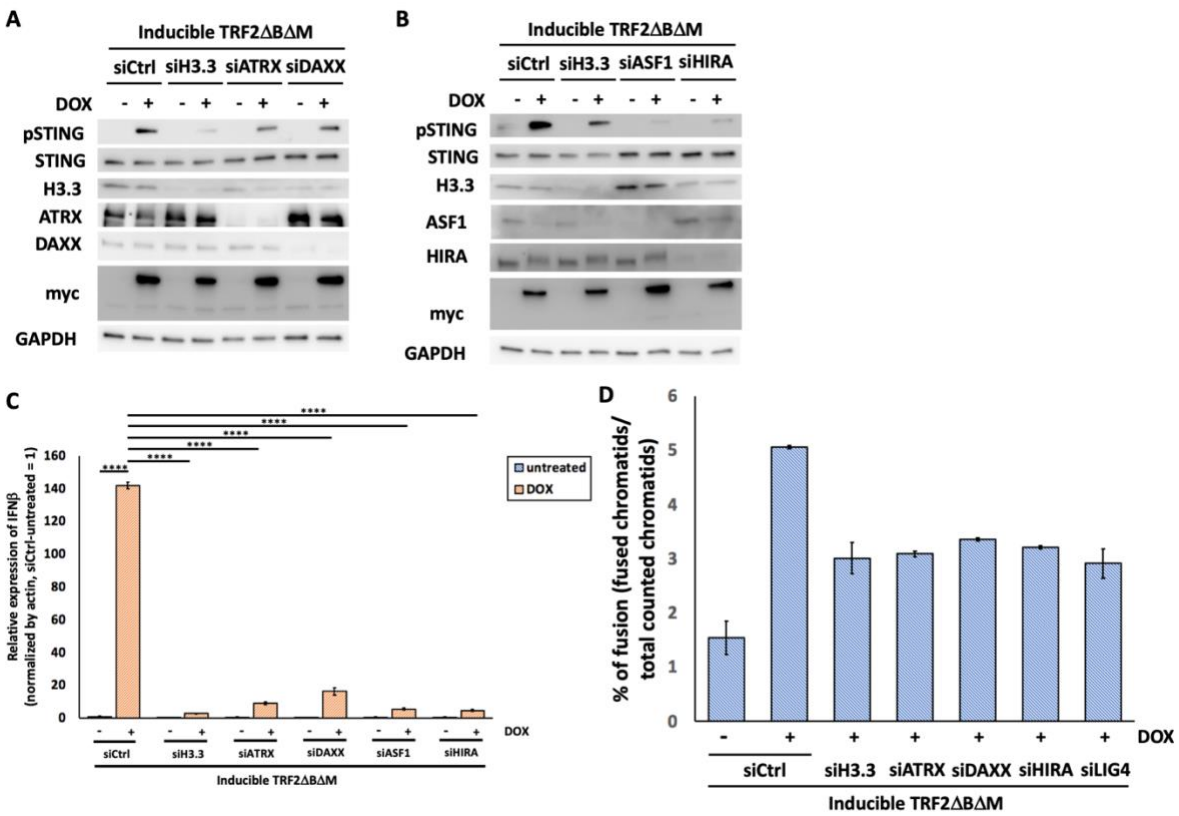

Figure 6. Depletion of H3.3 chaperones impairs cGAS-STING pathway activation. BJ^t cells were treated with siRNAs at 60 h and 12 h before inducing expression of myc-tagged TRF2ΔBΔM through DOX treatment. Samples were cultured for 2.5 days to investigate the cGAS-STING signaling response. (**A**, **B**) Protein levels of phosphorylated STING (pSTING), STING, ASF1, HIRA, ATRX, DAXX, H3.3, myc, and GAPDH were determined by Western blotting. (**C**) mRNA expression levels of IFNβ were determined by RT-qPCR. qPCR experiments represent the mean ±SD of three technical repeats. Another set of BJ^t cells was treated with siRNAs including siCtrl, siH3.3, siATRX, siDAXX, siHIRA, and siLIG4 at 60 h and 12 h before DOX treatment to induce expression of TRF2ΔBΔM for 24 h. Cells were arrested using 0.1 μg/ml Demecolcine for another 24 h, and then spread on a slide to visualize telomere fusion events by staining with a TelC probe. Statistical analysis was conducted using one-way ANOVA. **** p-value < 0.0001. (**D**) Quantitative results for telomere fusion events

were calculated from >2000 chromosomes for each sample. Data represent the mean ±SD of two sets of experiments.

REFERENCES

1. de Lange, T. (2018). Shelterin-Mediated Telomere Protection. Annu Rev Genet *52*, 223-247. 10.1146/annurev-genet-032918-021921.
2. Lundblad, V., and Szostak, J.W. (1989). A mutant with a defect in telomere elongation leads to senescence in yeast. Cell *57*, 633-643. 10.1016/0092-8674(89)90132-3.
3. van Steensel, B., Smogorzewska, A., and de Lange, T. (1998). TRF2 protects human telomeres from end-to-end fusions. Cell *92*, 401-413. 10.1016/s0092-8674(00)80932-0.
4. Karlseder, J., Smogorzewska, A., and de Lange, T. (2002). Senescence induced by altered telomere state, not telomere loss. Science *295*, 2446-2449. 10.1126/science.1069523.
5. Karlseder, J., Broccoli, D., Dai, Y., Hardy, S., and de Lange, T. (1999). p53- and ATM-dependent apoptosis induced by telomeres lacking TRF2. Science *283*, 1321-1325. 10.1126/science.283.5406.1321.
6. Xu, Y., and Baltimore, D. (1996). Dual roles of ATM in the cellular response to radiation and in cell growth control. Genes Dev *10*, 2401-2410. 10.1101/gad.10.19.2401.
7. Carney, J.P., Maser, R.S., Olivares, H., Davis, E.M., Le Beau, M., Yates, J.R., 3rd, Hays, L., Morgan, W.F., and Petrini, J.H. (1998). The hMre11/hRad50 protein complex and Nijmegen breakage syndrome: linkage of double-strand break repair to the cellular DNA damage response. Cell *93*, 477-486. 10.1016/s0092-8674(00)81175-7.
8. Usui, T., Ogawa, H., and Petrini, J.H. (2001). A DNA damage response pathway controlled by Tel1 and the Mre11 complex. Mol Cell *7*, 1255-1266. 10.1016/s1097-2765(01)00270-2.
9. Celli, G.B., Denchi, E.L., and de Lange, T. (2006). Ku70 stimulates fusion of dysfunctional telomeres yet protects chromosome ends from homologous recombination. Nat Cell Biol *8*, 885-890. 10.1038/ncb1444.
10. Smogorzewska, A., Karlseder, J., Holtgreve-Grez, H., Jauch, A., and de Lange, T. (2002). DNA ligase IV-dependent NHEJ of deprotected mammalian telomeres in G1 and G2. Curr Biol *12*, 1635-1644. 10.1016/s0960-9822(02)01179-x.
11. Abdisalaam, S., Bhattacharya, S., Mukherjee, S., Sinha, D., Srinivasan, K., Zhu, M., Akbay, E.A., Sadek, H.A., Shay, J.W., and Asaithamby, A. (2020). Dysfunctional telomeres trigger cellular senescence mediated by cyclic GMP-AMP synthase. J Biol Chem *295*, 11144-11160. 10.1074/jbc.RA120.012962.
12. Khoo, L.T., and Chen, L.Y. (2018). Role of the cGAS-STING pathway in cancer development and oncotherapeutic approaches. EMBO Rep *19*. 10.15252/embr.201846935.
13. Maciejowski, J., Li, Y., Bosco, N., Campbell, P.J., and de Lange, T. (2015). Chromothripsis and Kataegis Induced by Telomere Crisis. Cell *163*, 1641-1654. 10.1016/j.cell.2015.11.054.
14. Erdal, E., Haider, S., Rehwinkel, J., Harris, A.L., and McHugh, P.J. (2017). A prosurvival DNA damage-induced cytoplasmic interferon response is mediated by end resection factors and is limited by Trex1. Genes Dev *31*, 353-369. 10.1101/gad.289769.116.

531 15. Chen, Y.A., Shen, Y.L., Hsia, H.Y., Tiang, Y.P., Sung, T.L., and Chen, L.Y. (2017).
532 Extrachromosomal telomere repeat DNA is linked to ALT development via cGAS-
533 STING DNA sensing pathway. Nat Struct Mol Biol *24*, 1124-1131.
534 10.1038/nsmb.3498.
535 16. Lv, N., Zhao, Y., Liu, X., Ye, L., Liang, Z., Kang, Y., Dong, Y., Wang, W., Kolliputi, N., and
536 Shi, L. (2022). Dysfunctional telomeres through mitostress-induced cGAS/STING
537 activation to aggravate immune senescence and viral pneumonia. Aging Cell *21*,
538 e13594. 10.1111/acel.13594.
539 17. Wong, L.H., McGhie, J.D., Sim, M., Anderson, M.A., Ahn, S., Hannan, R.D., George,
540 A.J., Morgan, K.A., Mann, J.R., and Choo, K.H. (2010). ATRX interacts with H3.3 in
541 maintaining telomere structural integrity in pluripotent embryonic stem cells.
542 Genome Res *20*, 351-360. 10.1101/gr.101477.109.
543 18. Goldberg, A.D., Banaszynski, L.A., Noh, K.M., Lewis, P.W., Elsaesser, S.J., Stadler, S.,
544 Dewell, S., Law, M., Guo, X., Li, X., et al. (2010). Distinct factors control histone
545 variant H3.3 localization at specific genomic regions. Cell *140*, 678-691.
546 10.1016/j.cell.2010.01.003.
547 19. Drane, P., Ouararhni, K., Depaux, A., Shuaib, M., and Hamiche, A. (2010). The death-
548 associated protein DAXX is a novel histone chaperone involved in the replication-
549 independent deposition of H3.3. Genes Dev *24*, 1253-1265. 10.1101/gad.566910.
550 20. Armache, A., Yang, S., Martinez de Paz, A., Robbins, L.E., Durmaz, C., Cheong, J.Q.,
551 Ravishankar, A., Daman, A.W., Ahimovic, D.J., Klevorn, T., et al. (2020). Histone H3.3
552 phosphorylation amplifies stimulation-induced transcription. Nature *583*, 852-857.
553 10.1038/s41586-020-2533-0.
554 21. Ishiuchi, T., Abe, S., Inoue, K., Yeung, W.K.A., Miki, Y., Ogura, A., and Sasaki, H.
555 (2021). Reprogramming of the histone H3.3 landscape in the early mouse embryo.
556 Nat Struct Mol Biol *28*, 38-49. 10.1038/s41594-020-00521-1.
557 22. Huang, X.W., Cheng, X.R., Wang, N., Zhang, Y.W., Liao, C., Jin, L.H., and Lei, L. (2018).
558 Histone variant H3.3 and its functions in reprogramming. Yi Chuan *40*, 186-196.
559 10.16288/j.yczz.17-233.
560 23. Loppin, B., and Berger, F. (2020). Histone Variants: The Nexus of Developmental
561 Decisions and Epigenetic Memory. Annu Rev Genet *54*, 121-149. 10.1146/annurev-
562 genet-022620-100039.
563 24. Alvarez-Astudillo, F., Garrido, D., Varas-Godoy, M., Gutierrez, J.L., Villanueva, R.A.,
564 and Loyola, A. (2021). The histone variant H3.3 regulates the transcription of the
565 hepatitis B virus. Ann Hepatol *21*, 100261. 10.1016/j.aohep.2020.09.005.
566 25. Bockaj, I., Martini, T.E.I., de Camargo Magalhaes, E.S., Bakker, P.L., Meeuwsen-de
567 Boer, T.G.J., Armandari, I., Meuleman, S.L., Mondria, M.T., Stok, C., Kok, Y.P., et al.
568 (2021). The H3.3K27M oncohistone affects replication stress outcome and provokes
569 genomic instability in pediatric glioma. PLoS Genet *17*, e1009868.
570 10.1371/journal.pgen.1009868.
571 26. Voon, H.P.J., Hii, L., Garvie, A., Udugama, M., Krug, B., Russo, C., Chueh, A.C., Daly,
572 R.J., Morey, A., Bell, T.D.M., et al. (2023). Pediatric glioma histone H3.3 K27M/G34R
573 mutations drive abnormalities in PML nuclear bodies. Genome Biol *24*, 284.
574 10.1186/s13059-023-03122-5.
575 27. Haase, S., Banerjee, K., Mujeeb, A.A., Hartlage, C.S., Nunez, F.M., Nunez, F.J.,
576 Alghamri, M.S., Kadiyala, P., Carney, S., Barissi, M.N., et al. (2022). H3.3-G34

577 mutations impair DNA repair and promote cGAS/STING-mediated immune responses
578 in pediatric high-grade glioma models. J Clin Invest *132*. 10.1172/JCI154229.
579 28. Schwartzentruber, J., Korshunov, A., Liu, X.Y., Jones, D.T., Pfaff, E., Jacob, K., Sturm,
580 D., Fontebasso, A.M., Quang, D.A., Tonjes, M., et al. (2012). Driver mutations in
581 histone H3.3 and chromatin remodelling genes in paediatric glioblastoma. Nature
582 *482*, 226-231. 10.1038/nature10833.
583 29. Brosnan-Cashman, J.A., Yuan, M., Graham, M.K., Rizzo, A.J., Myers, K.M., Davis, C.,
584 Zhang, R., Esopi, D.M., Raabe, E.H., Eberhart, C.G., et al. (2018). ATRX loss induces
585 multiple hallmarks of the alternative lengthening of telomeres (ALT) phenotype in
586 human glioma cell lines in a cell line-specific manner. PLoS One *13*, e0204159.
587 10.1371/journal.pone.0204159.
588 30. Heaphy, C.M., de Wilde, R.F., Jiao, Y., Klein, A.P., Edil, B.H., Shi, C., Bettegowda, C.,
589 Rodriguez, F.J., Eberhart, C.G., Hebbar, S., et al. (2011). Altered telomeres in tumors
590 with ATRX and DAXX mutations. Science *333*, 425. 10.1126/science.1207313.
591 31. Ramamoorthy, M., and Smith, S. (2015). Loss of ATRX Suppresses Resolution of
592 Telomere Cohesion to Control Recombination in ALT Cancer Cells. Cancer Cell *28*,
593 357-369. 10.1016/j.ccell.2015.08.003.
594 32. Jiao, Y., Killela, P.J., Reitman, Z.J., Rasheed, A.B., Heaphy, C.M., de Wilde, R.F.,
595 Rodriguez, F.J., Rosemberg, S., Oba-Shinjo, S.M., Nagahashi Marie, S.K., et al. (2012).
596 Frequent ATRX, CIC, FUBP1 and IDH1 mutations refine the classification of malignant
597 gliomas. Oncotarget *3*, 709-722. 10.18632/oncotarget.588.
598 33. Koschmann, C., Calinescu, A.A., Nunez, F.J., Mackay, A., Fazal-Salom, J., Thomas, D.,
599 Mendez, F., Kamran, N., Dzaman, M., Mulpuri, L., et al. (2016). ATRX loss promotes
600 tumor growth and impairs nonhomologous end joining DNA repair in glioma. Sci
601 Transl Med *8*, 328ra328. 10.1126/scitranslmed.aac8228.
602 34. Dyer, M.A., Qadeer, Z.A., Valle-Garcia, D., and Bernstein, E. (2017). ATRX and DAXX:
603 Mechanisms and Mutations. Cold Spring Harb Perspect Med *7*.
604 10.1101/cshperspect.a026567.
605 35. Haase, S., Garcia-Fabiani, M.B., Carney, S., Altshuler, D., Nunez, F.J., Mendez, F.M.,
606 Nunez, F., Lowenstein, P.R., and Castro, M.G. (2018). Mutant ATRX: uncovering a
607 new therapeutic target for glioma. Expert Opin Ther Targets *22*, 599-613.
608 10.1080/14728222.2018.1487953.
609 36. Shi, L., Wen, H., and Shi, X. (2017). The Histone Variant H3.3 in Transcriptional
610 Regulation and Human Disease. J Mol Biol *429*, 1934-1945.
611 10.1016/j.jmb.2016.11.019.
612 37. Luijsterburg, M.S., de Krijger, I., Wiegant, W.W., Shah, R.G., Smeenk, G., de Groot,
613 A.J.L., Pines, A., Vertegaal, A.C.O., Jacobs, J.J.L., Shah, G.M., and van Attikum, H.
614 (2016). PARP1 Links CHD2-Mediated Chromatin Expansion and H3.3 Deposition to
615 DNA Repair by Non-homologous End-Joining. Mol Cell *61*, 547-562.
616 10.1016/j.molcel.2016.01.019.
617 38. Hopfner, K.P., and Hornung, V. (2020). Molecular mechanisms and cellular functions
618 of cGAS-STING signalling. Nat Rev Mol Cell Biol *21*, 501-521. 10.1038/s41580-020-
619 0244-x.
620 39. Stetson, D.B., and Medzhitov, R. (2006). Recognition of cytosolic DNA activates an
621 IRF3-dependent innate immune response. Immunity *24*, 93-103.
622 10.1016/j.immuni.2005.12.003.

623 40. Cesare, A.J., and Griffith, J.D. (2004). Telomeric DNA in ALT cells is characterized by
624 free telomeric circles and heterogeneous t-loops. Mol Cell Biol *24*, 9948-9957.
625 10.1128/MCB.24.22.9948-9957.2004.
626 41. Nabetani, A., and Ishikawa, F. (2009). Unusual telomeric DNAs in human telomerase-
627 negative immortalized cells. Mol Cell Biol *29*, 703-713. 10.1128/MCB.00603-08.
628 42. Cesare, A.J., and Reddel, R.R. (2008). Telomere uncapping and alternative
629 lengthening of telomeres. Mech Ageing Dev *129*, 99-108.
630 10.1016/j.mad.2007.11.006.
631 43. Celli, G.B., and de Lange, T. (2005). DNA processing is not required for ATM-
632 mediated telomere damage response after TRF2 deletion. Nat Cell Biol *7*, 712-718.
633 10.1038/ncb1275.
634 44. Pampalona, J., Soler, D., Genesca, A., and Tusell, L. (2010). Telomere dysfunction and
635 chromosome structure modulate the contribution of individual chromosomes in
636 abnormal nuclear morphologies. Mutat Res *683*, 16-22.
637 10.1016/j.mrfmmm.2009.10.001.
638 45. Takaki, T., Millar, R., Hiley, C.T., and Boulton, S.J. (2024). Micronuclei induced by
639 radiation, replication stress, or chromosome segregation errors do not activate
640 cGAS-STING. Mol Cell *84*, 2203-2213 e2205. 10.1016/j.molcel.2024.04.017.
641 46. Dimitrova, N., and de Lange, T. (2009). Cell cycle-dependent role of MRN at
642 dysfunctional telomeres: ATM signaling-dependent induction of nonhomologous end
643 joining (NHEJ) in G1 and resection-mediated inhibition of NHEJ in G2. Mol Cell Biol
644 *29*, 5552-5563. 10.1128/MCB.00476-09.
645 47. Malaquin, N., Olivier, M.A., Martinez, A., Nadeau, S., Sawchyn, C., Coppe, J.P.,
646 Cardin, G., Mallette, F.A., Campisi, J., and Rodier, F. (2020). Non-canonical ATM/MRN
647 activities temporally define the senescence secretory program. EMBO Rep *21*,
648 e50718. 10.15252/embr.202050718.
649 48. Grover, P., Asa, J.S., and Campos, E.I. (2018). H3-H4 Histone Chaperone Pathways.
650 Annu Rev Genet *52*, 109-130. 10.1146/annurev-genet-120417-031547.
651 49. Sturm, D., Witt, H., Hovestadt, V., Khuong-Quang, D.A., Jones, D.T., Konermann, C.,
652 Pfaff, E., Tonjes, M., Sill, M., Bender, S., et al. (2012). Hotspot mutations in H3F3A
653 and IDH1 define distinct epigenetic and biological subgroups of glioblastoma. Cancer
654 Cell *22*, 425-437. 10.1016/j.ccr.2012.08.024.
655 50. Udugama, M., Hii, L., Garvie, A., Cervini, M., Vinod, B., Chan, F.L., Das, P.P., Mann,
656 J.R., Collas, P., Voon, H.P.J., and Wong, L.H. (2021). Mutations inhibiting KDM4B
657 drive ALT activation in ATRX-mutated glioblastomas. Nat Commun *12*, 2584.
658 10.1038/s41467-021-22543-z.
659 51. Elbakry, A., Juhasz, S., Chan, K.C., and Lobrich, M. (2021). ATRX and RECQ5 define
660 distinct homologous recombination subpathways. Proc Natl Acad Sci U S A *118*.
661 10.1073/pnas.2010370118.
662 52. Cleal, K., Norris, K., and Baird, D. (2018). Telomere Length Dynamics and the
663 Evolution of Cancer Genome Architecture. Int J Mol Sci *19*. 10.3390/ijms19020482.
664 53. Capper, R., Britt-Compton, B., Tankimanova, M., Rowson, J., Letsolo, B., Man, S.,
665 Haughton, M., and Baird, D.M. (2007). The nature of telomere fusion and a definition
666 of the critical telomere length in human cells. Genes Dev *21*, 2495-2508.
667 10.1101/gad.439107.
668

REAGENT or RESOURCE	SOURCE	IDENTIFIER
Antibodies		
Phospho-STING (Ser366) (D7C3S)	Cell Signaling Technology	19781 RRID: AB_2737062
STING	R&D Systems	MAB7169 RRID: AB_1091940
cGAS	Cell Signaling Technology	15102 RRID: AB_2732795
H3.3	Milipore	09-838 RRID: AB_10845793
H3.3	Abcam	Ab176840 RRID: AB_2715502
myc	Sigma-Aldrich	M4439 RRID: AB_439694
LIG4	Proteintech	12695-1-AP RRID: AB_2136253
XRCC4	Proteintech	15817-1-AP RRID: AB_2257478
ATRX	Bethyl	A301-045A RRID: AB_2243144
DAXX	Bethyl	A301-353A RRID: AB_937792
HIRA	Milipore	04-1488 RRID: AB_1977097
ASF1	Santa Cruz Biotechnology	sc-53171 RRID: AB_2059662
Phosphor-Histone H2AX (Ser139)	Millipore	05-636 RRID: AB_309864
DAPI	Thermo Fisher Scientific	D1306
TRF1	GeneTex, customized	Customized, 90549
TRF2	GeneTex, customized	Customized, 90550
HRP-conjugated GAPDH	ProteinTech	HRP-60004 RRID: AB_2737588
HRP-conjugated beta-actin	ProteinTech	HRP-60008 RRID: AB_2819183
Mouse IgG Alexa Fluor 488	Thermo Fisher Scientific	A-11001 RRID: AB_2534069
Rabbit IgG Alexa Fluor 555	Thermo Fisher Scientific	A32727 RRID: AB_2633276
Chemicals, peptides, and recombinant proteins		
Mirin	Sigma-Aldrich	M9948
Doxycycline	TaKaRa	631311
Critical commercial assays		
Lipofectamine RNAiMAX Transfection Reagent	Invitrogen	13778075
TransIT-LT1	Mirus	MR-MIR2300
Mini-Rprotean TGX precast gels, 15 well	Bio-Rad	456-1096
ECL Western Blotting Detection kit	Millipore	NEL122001EA
Supersignal West Femto	Thermo	PIE 34096
NucleoSpin RNA, Mini kit for RNA purification	Macherey-Nagel	740955.50
iScript cDNA synthesis general supply	Bio-Rad	170-8891
ChIP Kit	Abcam	Ab500
Blocking reagent	Roche	10057177103

Experimental models: Cell lines		
BJ [Human fibroblast]	ATCC	RRID: CVCL-3653 CRL-2522
Oligonucleotides		
On-target plus siRNA reagent, siRNA sequences, see Table S1	Dharmacon	N/A
qRTPCR primers	This paper	Table S2
HPLC purified, >90% TMR-OO-ccctaaaccctaaaccctaaa probe	Panagene, customized	Customized
Software and algorithms		
ImageJ	ImageJ	http://imagej.net/ij/
Prism 9	GraphPad	http://www.graphpad.com/
Imaging systems		
Axio Imager Z1 System	Zeiss	N/A
ImageXpress Micro XLS System	Molecular Devices	N/A
DeltaVision Deconvolution Microscope	Image Solutions	N/A

Materials and Methods

Cell lines

Cell lines were obtained from ATCC and maintained under their recommended culturing conditions. BJ^t cells originated from BJ normal fibroblasts that stably express hTERT. The retroviral transformation was performed to generate cells that inducibly express green fluorescence protein (GFP), the TRF2 mutant TRF2ΔBΔM, or the TPP1 mutant TPP1ΔRD. Cells were tested for target protein expression by treating with a minimum of 25 ng/ml of doxycycline.

Gene silencing

The siRNAs used were On-target plus siRNA reagents (Dharmacon). The siRNA reagents were generated using the SMARTselection algorithm, with chemical modifications to eliminate off-target effects. Four siRNAs for each of H3F3A, H3F3B, cGAS, LIG4, XRCC4, ATRX, DAXX, HIRA, ASF1A, and ASF1B, as well as two siRNAs for NBS1, were employed. siRNAs were transfected into the cells using Lipofectamine RNAiMAX (Invitrogen) according to the manufacturer's instructions. Depletion of H3.3 and ASF1 was performed by mixing equal amounts of siRNAs targeting H3.3 and ASF1. MRN chemical inhibitors, Mirin (M9948, Sigma), was dissolved in DMSO as 10mM stock, and treated to the cell culture at the indicated concentrations.

Protein extraction, Western blots, and antibodies

Cell extracts were harvested using 1 X SDS sample buffer (62.5 mM Tris, pH 6.8, 10% glycerol, 2% SDS, 0.01% bromophenol blue, and 10% β-mercaptoethanol). Proteins were denatured by

698 heating the extract at 95 °C for 10 minutes. Proteins were separated by SDS-PAGE, and
699 transferred to a nitrocellulose membrane. The membranes were blocked with either Tris-
700 buffered saline (TBS) at pH 8.0 with 5% milk and 0.1% Tween-20 to determine phosphorylated
701 proteins or using Phosphate-buffered saline (PBS) at pH 8.0 with 5% milk and 0.1% Tween-20
702 to determine other proteins. Primary antibodies including phosphorylated STING (19781, Cell
703 Signaling), STING (MAB7169, R&D Systems), cGAS (15102, Cell Signaling), H3.3 (09-838,
704 Merkmillpore; ab176840, Abcam), myc (M4439, Sigma), LIG4 (12695-1-AP, Proteintech),
705 XRCC4 (15817-1-AP, Proteintech), ATRX (A301-045A, Bethyl), DAXX (A301-353A, Bethyl), HIRA
706 (04-1488, Millipore), and ASF1 (sc-53171, Santa Cruz Biotechnology) were used at 1:1000
707 dilution. Horseradish peroxidase-conjugated secondary antibodies were used at 1:2000
708 dilution to determine the proteins in the samples. As an internal control for gene expression,
709 HRP-conjugated GAPDH antibody (HRP60004, ProteinTech) and HRP-labeled ACTB (HRP-60008,
710 ProteinTech) were used at 1:5000 dilution. Either enhanced chemiluminescence (ECL) or
711 SuperSignal West Femto Maximum Sensitivity reagents (Thermo Fisher Scientific) were used
712 for signal detection.
713
714 RNA extraction and quantitative real-time PCR
715
716 Cells were lysed and harvested to extract total RNA using an RNA Mini Kit (Macherey-Nagel).
717 Reverse transcription was performed with iScript Reverse Transcriptase Supermix (Bio-Rad) to
718 generate cDNA for quantitative analyses. Quantitative real-time PCR was performed using
719 SYBR Green Select reagent (LifeTechnologies) to determine expression levels of target genes.
720 Quantitative PCR analysis was performed using a QuantStudio 12K Flex Real-Time PCR System
721 (ThermoFisher Scientific). The primer sequences are as follows: β-actin, 5'-
722 AGCACTGTGTTGGCGTACAG-3' and 5'-TCCCTGGAGAAGAGCTACGA-3'; interferon β, 5'-
723 AAACTCATGAGCAGTCTGCA-3' and 5'-AGGAGATCTTCAGTTTCGGAGG-3'. Data analysis was
724 performed by calculating the comparative Ct (ΔΔCt) of target genes normalized to an internal
725 control (β-actin).
726
727 Metaphase spread and telomere FISH on chromosomes
728
729 Analysis of telomere-to-telomere fusion was performed in DOX-treated cells subjected to
730 siRNA-mediated gene expression depletion. Cells were treated with DOX for 30 hours, and
731 reseeded in 0.1 μg/ml Demecolcine-containing medium. After 18 h of incubation, the floating
732 and attached cells were collected for further analysis. Cells were incubated with 75 mM KCl for
733 15 mins at 37 °C and routinely mixed at 5-minute intervals. Following KCl incubation, the cells
734 were fixed with fixing buffer (3:1 methanol: acetic acid) at 4 °C for more than 24 h. Fixed cells
735 were dropped on a glass slide from a height of 20 cm, heated at 75 °C for 1 min, and then dried
736 at room temperature overnight. The slides were stained according to a standard fluorescence
737 in situ hybridization (FISH) FISH protocol. In brief, the slides were fixed with 10% formalin for
738 2 mins, and then dehydrated by incubating them in increasing percentages of ethanol solution.
739 The slides were dried and incubated with a probe mixture (70% formamide, 0.5% blocking
740 reagent (Roche), 250 nM TMR-conjugated (CCCTAA)3-PNA probe, 10 mM Tris pH 7.4) at 80 °C
741 for 3 mins. The slides were hybridized at room temperature in the dark for 3 h. Serial wash
742 steps were then performed, including twice with Wash I (70% formamide, 10 mM Tris-HCl pH
743 7.5), and twice with Wash II (100 mM Tris-HCl pH 7.5, 150 mM NaCl, 0.08% Tween-20). The
744 slides were counterstained with DAPI, dehydrated with ethanol, and mounted with

745 Fluoromount Aqueous Mounting Medium (Sigma). Images were acquired with a Zeiss Axio
746 Imager Z1 System. Determination and quantitative analysis of telomere fusion events were
747 performed by counting for 700 to 1500 chromosome pairs.
748
749 Immunofluorescence staining
750
751 Cells grown on coverslips were treated with permeabilization solution (20 mM Hepes pH 8.0,
752 50 mM NaCl, 3 mM MgCl2, 0.5% Triton-X 100, 300 mM sucrose), and fixed with 2%
753 paraformaldehyde. The cells were permeabilized with 0.5% Triton-X 100, and then blocked
754 with 2% fetal bovine serum (FBS) in phosphate-buffered saline. Primary antibodies including
755 anti-TRF1 (90549, GeneTex) and anti-γH2AX (05-636, Millipore) were used. The secondary
756 antibodies were Mouse IgG Alexa Fluor 488 (A-11001, Thermo Fisher Scientific) and Rabbit IgG
757 Alexa Fluor 555 (A32727, Thermo Fisher Scientific). The cells were stained with DAPI,
758 dehydrated, and mounted with ProLong Gold Antifade Mountant (Life Technologies). Images
759 were acquired under a DeltaVision Deconvolution Microscope. Colocalization events were
760 determined based on the overlapping of signals from different channels, and quantification
761 was performed by counting for > 100 nuclei on one coverslip.
762
763 Chromatin immunoprecipitation (ChIP)
764
765 The chromatin immunoprecipitation protocol was adapted from the Abcam ChIP kit (Ab500).
766 After depletion of gene expression by siRNAs for 4 days, the BJ^t cells were fixed with 1%
767 formaldehyde for 10 min. The cross-linking process was quenched with glycine, and the cells
768 were collected from the culture dish. Chromatin DNA was extracted from cells, and sheared
769 into 200-500 bp. Sheared chromatin DNAs were immunoprecipitated with antibodies,
770 including H3.3 (09-838, Merkmillpore) and TRF2 (90550, GeneTex) antibodies. Antibody-
771 precipitated chromatin DNAs were enriched with protein A beads. The enriched chromatin
772 DNAs were reversed crosslinking with protease and extracted from the precipitated DNA pellet.
773 Precipitated DNAs were then loaded on the Hybond-XL membrane. The telomeric DNA from
774 each sample was determined with α-P32-dCTP-labelled telomere probe.
775
776 Cell growth and quantification of nuclear abnormalities
777
778 Cell growth was determined by counting cells in the multi-well culture plates. Cells were plated
779 in 12-well plates and fixed with 2% paraformaldehyde on the 1st-7th days post-treatment. The
780 cells were stained with DAPI and imaged using an ImageXpress Micro XLS System (Molecular
781 Devices). For each well, images in 64 fixed regions were taken to quantify the number of cells
782 inside the well. These images were used to quantify nuclear abnormalities, including
783 nucleoplasmic bridges, nuclear buds, and micronuclei. Such abnormalities were identified
784 based on a deformed nuclear structure, and the quantification was performed by counting for
785 >2000 nuclei in one sample.
786
787 Quantification and statistical analysis
788
789 With the help of GraphPad Prism, a one-way analysis of variance (ANOVA) was performed to
790 assess the statistical differences among group means. Following a significant ANOVA result
791 ($P<0.05$), post-hoc comparisons were conducted using Tukey's Honest Significant Difference

792 (HSD) test to determine pairwise difference between group means and to control for Type I
793 error due to multiple comparisons.
794